Reactivity of $Co^+(^3F,^5F)$, $Ni^+(^2D,^4F)$, and $Cu^+(^1S,^3D)$: Reaction of Co^+, Ni^+, and Cu^+ with Water

Arantxa Irigoras, Oihana Elizalde, Iñaki Silanes, Joseph E. Fowler, and Jesus M. Ugalde*

Contribution from the Kimika Fakultatea, Euskal Herriko Unibertsitatea, P.K. 1072, 20080 Donostia, Euskadi, Spain

Received May 18, 1999. Revised Manuscript Received September 22, 1999

Abstract: In this paper we conclude the study of the reaction of water with the first row transition metal ions. We report the study of the reaction of water with the late (Co^+, Ni^+, and Cu^+) first row transition metal cations in both high- and low-spin states. In agreement with experimental observations, no exothermic products are found and the oxides are predicted to be more reactive than the metal ions. Formation of endothermic products is examined. An in-depth analysis of the reaction paths possible for these reactions is given, including various minima and several important transition states. All results have been compared with existing experimental and theoretical data, and our earlier works covering the (Sc^+-Fe^+) + H_2O reactions to observe existent trends for the first row transition metal ions.

1. Introduction

With the results reported in this work we finish a series of works on the reactivity of first row transition metal cations with water[1−4] with the aim of understanding this paradigm for the reactivity of these metal cations and their oxides. Previously, we have discussed the importance of both high- and low-spin potential energy surfaces, their particular features, and the spin-forbidden crossings that they involve. For the early (Sc, Ti, and V) and middle (Cr and Mn) transition metal cations the high-spin state was the one corresponding to the ground state, while the low-spin state was the ground state for their oxides. The iron cation presented a high-spin ground state, but its oxide also has a high-spin ground state, resulting in a very complicated two-state-specific reactivity. In the late transition metals we have in the ground states low-spin metal cations and high-spin metal oxide cations.

As we pointed out in our previous paper regarding the middle transition metal reactivity, the reactivity of these metals was studied by Kang and Beauchamp[5,6] in 1986. Based on the bond dissociation energies of the metal oxide cations they pointed out that the early MO^+ molecules (Sc, Ti, V) were too stable to react exothermically with alkenes as their dissociation energies are significantly larger than the ones corresponding to the Mn−Ni oxides, which are very reactive, the low dissociation energies leading to the possibility of exothermic processes. Cr was somewhat between these two different behaviors, exhibiting a balance in being reactive but selective. They also pointed out that exothermic thermochemistry does not ensure a facile reaction, but that a number of examples support the contention that barriers in exothermic reactions of transition metal oxide ions are rare.[5]

Several groups have developed a large body of work around the reactivity of these transition metals showing that the behavior of these systems is much more complicated than expected. In 1994 Schröder et al.[7] observed very low reactivities for the reactions of FeO^+, CoO^+, and NiO^+ with H_2. They surprisingly found that while CoO^+ has a binding energy close to that of FeO^+, and the binding energy of NiO^+ is much smaller, their $MO^+ + H_2$ reaction rates are very similar, and give rise to the exclusive formation of water and M^+.

Armentrout's group[8] also studied these reactions in both directions for the cobalt system. They observe a 0.75 ± 0.04 eV activation barrier for the exothermic oxidation of D_2 by CoO^+, probably attributable to a four-centered TS associated with addition of D−D across the CoO^+ bond. They observe two products in the oxidation of Co^+, the CoD^+ and $CoOD^+$ species, but no evidence of CoO^+ formation was observed in their study, a process that is thermochemically less endothermic than the ones giving rise to the two other products observed.

Fiedler et al.[9] postulate some generalities on the reactivity patterns of CoO^+, NiO^+, and CuO^+ with the hydrogen molecule based on their detailed theoretical study of the iron system, and experimental study of the reactions of CoO^+ with hydrogen, methane, and small alkanes.[10] They highlighted a low stabilization energy potential energy surface, where the high-spin surface must surmount a significant barrier in addition to the spin-inversion requirement, giving an explanation of the low efficiencies of these reactions in spite of the favorable thermochemistry.

As it was concluded in a review by Schröder and Schwarz,[11] despite favorable thermochemistry for the reaction of middle and late metal oxide cations with hydrogen molecule, only the

(1) Irigoras, A.; Ugalde, J. M.; Lopez, X.; Sarasola, C. *Can. J. Chem.* **1996**, *74*, 1824−1829.
(2) Irigoras, A.; Fowler, J. E.; Ugalde, J. M. *J. Phys. Chem. A* **1998**, *102*, 293, 2252.
(3) Irigoras, A.; Fowler, J. E.; Ugalde, J. M. *J. Am. Chem. Soc.* **1999**, *121*, 574.
(4) Irigoras, A.; Fowler, J. E.; Ugalde, J. M. *J. Am. Chem. Soc.* Submitted for publication.
(5) Kang, H.; Beauchamp, J. L. *J. Am. Chem. Soc.* **1986**, *108*, 5663.
(6) Kang, H.; Beauchamp, J. L. *J. Am. Chem. Soc.* **1986**, *108*, 7502.
(7) Schröder, D.; Fiedler, A.; Ryan, M. F.; Schwarz, H. *J. Phys. Chem.* **1994**, *98*, 68.
(8) Chen, Y.-M.; Clemmer, D. E.; Armentrout, P. B. *J. Am. Chem. Soc.* **1994**, *116*, 7815.
(9) Fiedler, A.; Schröder, D.; Shaik, S.; Schwarz, H. *J. Am. Chem. Soc.* **1994**, *116*, 10734.
(10) Ryan, M. F.; Fiedler, A.; Schröder, D.; Schwarz, H. *Organometallics* **1994**, *13*, 4072.
(11) Schröder, D.; Schwarz, H. *Angew. Chem., Int. Ed. Engl.* **1995**, *34*, 1973.

10.1021/ja991657r CCC: $19.00
Published on Web 12/22/1999

Table 1. Total Energies (E), in Hartree, Zero-Point Vibrational Energy Corrections (ΔZPVE), Basis Set Superposition Error Corrections (BSSE), and Dissociation Energies (D_0), in eV, for the $M(OH_2)^+$ Ion−Molecule Complexes (M = Co, Ni, Cu)

M	method	E	ΔZPVE	BSSE	D_0
Co	B3LYP/DZVP	−1458.72473	0.069	0.104	1.664
	B3LYP/TZVP+G(3df,2p)	−1459.00896	0.065	0.025	1.637
	CCSD(T)//B3LYP	−1458.04010	0.065	0.079	1.514
	expt[39,b]				**1.67 ± 0.06**
	expt[40,a]				1.610 ± 0.13
	expt[41,a]				1.740 ± 0.174
	theor[36] MCPF/[8s6p4d1f]				1.658
	theor[37] QCISD(T)/[8s6p4d1f]				1.575
	theor[38] CCSD(T)(FULL)/6-311++G(d,p)[c]				1.610
Ni	B3LYP/DZVP	−1584.24268	0.056	0.103	1.861
	B3LYP/TZVP+G(3df,2p)	−1584.57010	0.061	0.026	1.823
	CCSD(T)//B3LYP	−1583.56652	0.061	0.080	1.690
	expt[39,b]				**1.87 ± 0.03**
	expt[40,a]				1.584 ± 0.13
	expt[41,a]				1.723 ± 0.174
	theor[36] MCPF/[8s6p4d1f]				1.784
	theor[37] QCISD(T)/[8s6p4d1f]				1.672
	theor[38] CCSD(T)(FULL)/6-311++G(d,p)[c]				1.575
Cu	B3LYP/DZVP	−1716.40775	0.061	0.126	1.784
	B3LYP/TZVP+G(3df,2p)	−1716.77247	0.065	0.040	1.653
	CCSD(T)//B3LYP	−1715.72612	0.065	0.101	1.452
	expt[39,b]				**1.63 ± 0.08**
	expt[40,a]				1.519 ± 0.13
	expt[41,a]				1.424 ± 0.174
	theor[36] MCPF/[8s6p4d1f]				1.619
	theor[37] QCISD(T)/[8s6p4d1f]				1.559
	theor[38] CCSD(T)(FULL)/6-311++G(d,p)[c]				1.567

[a] Temperature not specified. [b] Values at 0 K. [c] Values at 298 K.

reaction of MnO^+ with H_2 is efficient; CrO^+, CoO^+, and NiO^+ hardly react and the reaction of FeO^+ occurs only rarely. These reactions must be controlled by reaction barriers and the ease of curve crossing from the high-spin ground states of MO^+ to the low-spin surface.

No experimental data are available for the copper system as it seems that CuO^+ cannot be generated in reasonable quantities,[11] but a low efficiency is expected for the ground-state high-spin copper oxide in the reaction $CuO^+ + H_2 \rightarrow Cu^+ + H_2O$.[9]

Seeing that there exists an interest in the reactivities of the entire series of first row transition metals, we here complete our goal of providing high- and low-spin potential energy surfaces for their reactions with water. We present, as usual, the full reaction mechanism geometries and energetics for both the high- and low-spin states, considering the various possible transition states, intermediates, and products.

2. Methods

The experience of this group[1−4] shows that Density Functional Theory (B3LYP functional)[12−16] with the DZVP basis sets given by Salahub et al.[17,18] is a reasonable choice for optimization and frequency calculations of these systems. The choice of the B3LYP functional is largely motivated by its satisfactory performance reported recently[19−26] for transition metal containing systems. Reactants and products of the possible reactions have also been reoptimized at the B3LYP/TZVP+G(3df,2p) level of theory. All the calculations have been corrected with the Zero Point Vibrational Energy (ZPVE) calculated at the corresponding theoretical level.

To confirm the B3LYP results, some single point CCSD(T)/TZVP+G(3df,2p) calculations have been carried out at the B3LYP/TZVP+G(3df,2p) equilibrium geometries. The 1s electrons of O and 1s to 2p electrons of the metals were frozen in the CCSD(T) calculations. For the sake of brevity, on occasion in this article we will abreviate CCSD(T)/TZVP+G(3df,2p)//B3LYP/TZVP+G(3df,2p) as CCSD(T)//B3LYP.

The triple-ζ quality basis set, TZVP+G(3df,2p), used for the metals was that given by Schäfer, Hubert, and Ahlrichs,[27] supplemented with a diffuse s function (with an exponent 0.33 times that of the most diffuse s function on the original set), two sets of p functions optimized by Wachters[28] for the excited states, one set of diffuse pure angular momentum d function (optimized by Hay),[29] and three sets of uncontracted pure angular momentum f functions, including both tight and diffuse exponents, as recommended by Ragavachari and Trucks.[30] For the oxygen and hydrogen atoms the 6-311++G(2df,2p) basis set of Pople et al.[31] was used.

All DFT and CCSD(T) calculations reported in this paper have been carried out with the GAUSSIAN94/DFT[32] and GAUSSIAN98/DFT[33] suites of programs. Also Natural Bonding Orbital (NBO)[34,35] calculations have been done to give additional insight into the bonding properties of some of the structures.

3. Results and Discussion

3.1. Dissociation Energies. Dissociation energies of the $Co(OH_2)^+$, $Ni(OH_2)^+$, and $Cu(OH_2)^+$ ion−molecules calculated at the B3LYP/DZVP, B3LYP/TZVP+G(3df,2p), and CCSD(T)//B3LYP levels of theory are shown in Table 1. Dissociation

(12) Becke, A. D. *Phys. Rev. A* **1988**, *38*, 3098.
(13) Becke, A. D. *J. Chem. Phys.* **1993**, *98*, 5648.
(14) Lee, C.; Yang, W.; Parr, R. G. *Phys. Rev. B* **1988**, *37*, 785.
(15) Miehlich, B.; Savin, A.; Stoll, H.; Preuss, H. *Chem. Phys. Lett.* **1989**, *157*, 200.
(16) Stephens, P. J.; Devlin, F. J.; Ashvar, C. S.; Chabalowski, C. F.; Frisch, M. J. *Faraday Discuss.* **1994**, *99*, 103. (b) Stephens, P. J.; Devlin, F. J.; Frisch, M. J.; Chabalowski, C. F. *J. Phys. Chem.* **1994**, *98*, 11623.
(17) Sim, F.; Salahub, D. R.; Chim, S.; Dupuis, M. *J. Chem. Phys.* **1991**, *95*, 4317.
(18) Godbout, N.; Salahub, D. R.: Andzelm, J.; Wimmer, E. *Can. J. Chem.* **1992**, *70*, 560.
(19) Bauschlicher, C. W., Jr.; Ricca, A.; Partridge, H.; Langhoff, S. R. *Recent Advances in Density Functional Theory*; Chong, D. P., Ed.; World Scientific Publishing Co.: Singapore, 1997; Part II.
(20) Filatov, M.; Shaik, S. *J. Phys. Chem. A* **1998**, *102*, 3835.
(21) Sodupe, M.; Branchadell, V.; Rosi, M.; Bauschlicher, C. W., Jr. *J. Phys. Chem. A* **1997**, *101*, 7854−7859.
(22) Siegbahn, P. E. M. Electronic structure calculations for molecules containing transition metals. *Adv. Chem. Phys.* **1996**, *43*.
(23) Ricca, A.; Bauschlicher, C. W. *J. Phys. Chem.* **1994**, *98*, 12899.
(24) Bauschlicher, C. W.; Maitre, P. *J. Phys. Chem.* **1995**, *99*, 3444.
(25) Hartmann, M.; Clark, T.; van Eldik, R. *J. Am. Chem. Soc.* **1997**, *119*, 7843.
(26) Pavlov, M.; Siegbahn, P. E. M.; Sandström, M. *J. Phys. Chem. A* **1998**, *102*, 219.
(27) Schäfer, A.; Hurbert, C.; Ahlrichs, R. *J. Chem. Phys.* **1994**, *100*, 5829.
(28) Wachters, A. J. *J. Chem. Phys.* **1970**, *52*, 1033.
(29) Hay, P. J. *J. Chem. Phys.* **1971**, *66*, 4377.
(30) Raghavachari, K.; Trucks, G. W. *J. Chem. Phys.* **1989**, *91*, 1062.
(31) Krishnan, J. S.; Binkley, J. S.; Seeger, P.v. R.; Pople, J. A. *J. Chem. Phys.* **1980**, *72*, 650.

energies were calculated as the difference between the energy of the isolated monomers and the complex, including both Basis Set Superposition Error (BSSE) and ZPVE corrections.

$M(OH_2)^+$ dissociation energies predicted by various levels of theory (MCPF/[8s6p4d1f] results, from Rosi and Bauschlicher,[36] QCISD(T) results from Magnusson and Moriarty,[37] and the recent CCSD(T)(FULL)/6-311++G**//MP2(FULL)/6-311++G** results from Trachtman et al.[38]) and those experimentally observed[39−41] are given also in Table 1. Note that the temperature is not specified in refs 40 and 41.

Once more, good values are obtained with both the B3LYP and CCSD(T) methods when used in conjunction with the TZVP+G(3df,2p) basis set.[1−4] The difference found between the B3LYP/DZVP and B3LYP/TZVP+G(3df,2p) results is again around 0.065 eV and both are in reasonable agreement with the experimental and theoretical values that can be found in Table 1, especially with the more recent and precise data from Armentrout's group.[39] The CCSD(T) values are systematically lower as is usual for dissociation energies.

The values listed for the $Co(OH_2)^+$ complex correspond to the $^3A_2$ ground state, in accordance with Trachtman et al.[38] but not with Rosi and Bauschlicher,[36] as they predict a $^3B_2$ ground state for this ion−molecule, with a geometry reasonably similar to ours. They predict that the $^3A_2$ excited state is only 0.030 eV higher in energy, while our $^3A_2$ state lies 0.091 eV lower in energy than the $^3B_2$ state at the CCSD(T)//B3LYP level of theory. In any case, these discrepancies at the various computational levels are not large and do not change the overall trend of the dissociation energies in comparison with experimental data.

In considering the results of this series of studies on the first row transition metals, examination of the mean deviations of the obtained values with respect to the values given by Armentrout's group[39] shows a very good agreement: a deviation of 0.08 eV at the B3LYP/DZVP level of theory, 0.05 eV at the B3LYP/TZVP+G(3df,2p) level, and 0.12 eV at the CCSD(T)//B3LYP level. It should be pointed out that while a tendency to overestimate has been observed at the B3LYP level, the CCSD(T) level underestimates the dissociation energies in all cases, except for the iron case where a perfect matching was obtained. These tendencies are those expected for the methods used. The method that best fits the experimental data is the B3LYP/TZVP+G(3df,2p) level of theory, all the values calculated are almost within the experimental error bar, the greatest discrepancy coming in the iron system, 0.08 eV vs the experimental error bars of 0.06 eV.

Table 2. Relative Energies, in eV, for the $^5F(sd^7)$ State of Co^+ with Respect to the $^3F(d^8)$ Ground State (Δ_1), the $^5B_2$ State of $Co(OH_2)^+$ with Respect to the $^3A_2$ Ground State (Δ_2), and the $^3\Sigma$ State of CoO^+ with Respect to the $^5\Delta$ Ground State (Δ_3)

method	Δ_1	Δ_2	Δ_3
B3LYP/DZVP	0.935	1.211	0.657
B3LYP/TZVP+G(3df,2p)	0.721	0.966	0.645
CCSD(T)//B3LYP	0.530	0.719	0.887
expt[50]	0.43		
theor[9]			1.0

Table 3. Relative Energies, in eV, for the $^4F(sd^8)$ State of Ni^+ with Respect to the $^2D(d^9)$ Ground State (Δ_1), the $^4A'$ State of $Ni(OH_2)^+$ with Respect to the $^2A_1$ Ground State (Δ_2), the $^2\Sigma$ State of NiO^+ with Respect to the $^4\Sigma$ Ground State (Δ_3), and the $^2\Delta$ State of NiO^+ with Respect to the $^4\Sigma$ Ground State (Δ_4)

method	Δ_1	Δ_2	Δ_3	Δ_4
B3LYP/DZVP	1.377	1.783	0.391	0.558
B3LYP/TZVP+G(3df,2p)	1.210	1.572	0.411	0.538
CCSD(T)//B3LYP	1.262	1.550	0.606	0.793
expt[50]	1.08			
theor[9]				1.3

Table 4. Relative Energies, in eV, for the $^3D(sd^9)$ State of Cu^+ with Respect to the $^1S(d^{10})$ Ground State (Δ_1), the $^3B_1$ State of $Cu(OH_2)^+$ with Respect to the $^1A_1$ Ground State (Δ_2), and the $^1\Delta$ State of CuO^+ with Respect to the $^3\Sigma$ Ground State (Δ_3)

method	Δ_1	Δ_2	Δ_3
B3LYP/DZVP	2.998	3.243	0.583
B3LYP/TZVP+G(3df,2p)	2.911	3.123	0.562
CCSD(T)//B3LYP	3.291	3.447	0.632
expt[50]	2.81		
theor[9]			1.4

3.2. Excitation Energy. Let us look now to the high-/low-spin relative energies of M^+, $M(OH_2)^+$, and MO^+ shown in Table 2 (M = Co), Table 3 (M = Ni), and Table 4 (M = Cu), and compare them with the values given for the other first row transition metal M^+, $M(OH_2)^+$, and MO^+ moieties.[2−4]

For the early and middle transition metal cations the calculated high-/low-spin splittings were always lower than the experimental ones, but for the late M^+ there is an inversion in the trend. Discounting the Fe^+ case, notably poorly described by the B3LYP method,[4,20,47−49] this change can be related to the fact that for the earlier transition metals the ground state of the cation is high spin, while the ground state of these last three

(32) Frisch, M. J.; Trucks, G. W.; Schlegel, H. B.; Gill, P. M. W.; Johnson, B. G.; Robb, M. A.; Cheeseman, J. R.; Keith, T. A.; Petersson, G. A.; Montgomery, J. A.; Raghavachari, K.; Al-Laham, M. A.; Zakrzewski, V. G.; Ortiz, J. V.; Foresman, J. B.; Croslowski, J.; Stefanov, B. B.; Nanayakkara, A.; Challacombe, M.; Peng, C. Y.; Ayala, P. Y.; Chen, W.; Wong, M. W.; Andres, J. L.; Replogle, E. S.; Gomperts, R.; Martin, R. L.; Fox, D. J.; Binkley, J. S.; Defrees, D. J.; Baker, J.; Stewart, J. P.; Head-Gordon, M.; Gonzalez, C.; Pople, J. A. *Gaussian 94* (Revision B.2); Gaussian, Inc.: Pittsburgh, PA, 1995.

(33) Frisch, M. J.; Trucks, G. W.; Schlegel, H. B.; Scuseria, G. E.; Robb, M. A.; Cheeseman, J. R.; Zakrzewski, V. G.; Montgomery, J. A.; Stratmann, R. E.; Burant, J. C.; Dapprich, S.; Millam, J. M.; Daniels, A. D.; Kudin, K. N.; Strain, M. C.; Farkas, O.; Tomasi, J.; Barone, V.; Cossi, M.; Cammi, R.; Mennucci, B.; Pomelli, C.; Adamo, C.; Clifford, S.; Ochterski, J.; Petersson, G. A.; Ayala, P. Y.; Cui, Q.; Morokuma, K.; Malick, D. K.; Rabuck, A. D.; Raghavachari, K.; Foresman, J. B.; Cioslowski, J.; Ortiz, J. V.; Stefanov, B. B.; Liu, G.; Liashenko, A.; Piskorz, P.; Komaromi, I.; Gomperts, R.; Martin, R. L.; Fox, D. J.; Keith, T.; Al-Laham, M. A.; Peng, C. Y.; Nanayakkara, A.; Gonzalez, C.; Challacombe, M.; Gill, P. M. W.; Johnson, B. G.; Chen, W.; Wong, M. W.; Andres, J. L.; Head-Gordon, M.; Replogle, E. S.; Pople, J. A. *Gaussian 98* (Revision A.5); Gaussian, Inc.: Pittsburgh, PA, 1998.

(34) Reed, A. E.; Curtiss, L. A.; Weinhold, F. *Chem. Rev.* **1988**, *88*, 899.

(35) NBO Version 3.1; Glendening, A. E.; Reed, A. E.; Carpenter, J. E.; Weinhold, F.

(36) Rosi, M.; Bauschlicher, C. W. *J. Chem. Phys.* **1989**, *90* (12), 7264; **1990**, *92* (3), 1876.

(37) Magnusson, E.; Moriarty, N. W. *J. Comput. Chem.* **1993**, *14* (8), 961.

(38) Trachtman, M.; Markham, G. D.; Glusker, J. P.; George, P.; Bock, C. W. *Inorg. Chem.* **1998**, *37*, 4421.

(39) Dalleska, N. F.; Honma, K.; Sunderlin, L. S. Armentrout, P. B. *J. Am. Chem. Soc.* **1994**, *116*, 3519.

(40) Magnera, T. F.; David, D. E.; Michl, J. *J. Am. Chem. Soc.* **1989**, *111*, 4100.

(41) Marinelli, P. J.; Squires, R. R. *J. Am. Chem. Soc.* **1989**, *111*, 4101.

(42) Clemmer, D. E.; Aristov, N.; Armentrout, P. B. *J. Phys. Chem.* **1993**, *97*, 544−552.

(43) Ryan, M. F.; Fiedler, A.; Schröder, D.; Schwarz, H. *J. Am. Chem. Soc.* **1995**, *117*, 2033.

(44) Clemmer, D. E.; Chen, Y.-M.; Khan, F. A.; Armentrout, P. B. *J. Phys. Chem.* **1994**, *98*, 6522.

(45) Schröder, D.; Schwarz, H.; Clemmer, D. E.; Chen, Y.-M.; Armentrout, P. B.; Baranov, V. I.; Böhme, D. K. *Int. J. Mass. Spec. Ion. Proc.* **1997**, *161*, 175.

(46) Danovich, D.; Shaik, S. *J. Am. Chem. Soc.* **1997**, *119*, 1773.

(47) Ricca, A.; Bauschlicher, C. W. *Theor. Chim. Acta* **1995**, *92*, 123.

(48) Ricca, A.; Bauschlicher, C. W. *J. Phys. Chem.* **1995**, *99*, 9003.

(49) Holthausen, M. C.; Fiedler, A.; Schwarz, H.; Koch, W. *J. Phys. Chem.* **1996**, *100*, 6236.

Table 5. Overall Energies for Reactions 1−8 at Several Levels of Theory[a]

method	ΔE_1	ΔE_2	ΔE_3	ΔE_4	ΔE_5	ΔE_6	ΔE_7	ΔE_8
B3LYP/DZVP	−2.054	−2.711	−5.038	−5.612	−2.070	−2.759	−3.082	−3.601
B3LYP/TZVP+G(3df,2p)	−2.069	−2.714	−4.982	−5.631	−2.043	−2.813	−3.127	−3.741
CCSD(T)//B3LYP	−1.989	−2.876	−4.921	−5.642	−2.103	−2.920	−3.234	−3.892
expt[51]	-1.78 ± 0.05				-2.01 ± 0.04		-3.14 ± 0.06	

[a] Energies given are in eV and for the various B3LYP levels of theory include ZPVE corrections calculated at the corresponding level of theory.

is low spin. Calculating the overall deviations from the experimental values[50] we determine that for all the row B3LYP/TZVP+G(3df,2p) and CCSD(T)//B3LYP levels of theory perform similarly, with respective overall deviations of 0.196 and 0.214 eV, a performance slightly better than the B3LYP/DZVP method, which has a deviation of 0.286 eV. We must point out the significant overestimation obtained at the CCSD(T)//B3LYP level for the Cu^+ $^1S-^3D$ splitting, and the poor B3LYP/TZVP+G(3df,2p) description of the Fe^+ $^4F \rightarrow {}^6D$ splitting.

For the $M(OH_2)^+$ ion−molecules low → high spin excitation energies we observe, continuing the trend shown by the M = Sc−Cr ion−molecules, that CCSD(T)//B3LYP gives smaller splittings than B3LYP. Note that an increased gap is observed for the copper ion−molecule.

Finally, we examine the metal oxide cation MO^+ molecule. While the CCSD(T)//B3LYP method predicted lower excitation energies for CrO^+ and MnO^+ than did the B3LYP method, it gives larger excitation energies for these three late metal oxide cations, in good accordance with the values obtained with the iron oxide and the early transition metal oxides. In general, the calculated gaps are smaller than the ones reported by Fiedler et al. Our predictions of lowest-lying high- and low-spin states agree with those of Fiedler et al. except for the NiO^+ doublet ground state. We obtain a $^2\Sigma$ doublet ground state with a $^2\Delta$ state lying 0.187 eV higher in energy. A $^2\Delta$ state has been assigned as the ground state in Fiedler's calculations, while they do not give a value for the $^2\Sigma$ state.

3.3. Reaction Energetics. 3.3.1. $Co^+(^3F) + H_2O$. Equations 1−8 represent the main ionic products observed in the reaction of $Co^+(^3F)$ with H_2O. The predicted ΔE energies are listed in Table 5 together with the values for reactions 1, 5, and 7 extracted from the available thermodynamical data,[51] and the estimation of Ryan et al.[10] for reaction 1.

$$Co^+(^3F) + H_2O \rightarrow CoO^+(^5\Delta) + H_2 + \Delta E_1 \quad (1)$$

$$Co^+(^3F) + H_2O \rightarrow CoO^+(^3\Sigma) + H_2 + \Delta E_2 \quad (2)$$

$$Co^+(^3F) + H_2O \rightarrow HCoO^+(^4A'') + H + \Delta E_3 \quad (3)$$

$$Co^+(^3F) + H_2O \rightarrow HCoO^+(^2A'') + H + \Delta E_4 \quad (4)$$

$$Co^+(^3F) + H_2O \rightarrow CoOH^+(^4A') + H + \Delta E_5 \quad (5)$$

$$Co^+(^3F) + H_2O \rightarrow CoOH^+(^2A') + H + \Delta E_6 \quad (6)$$

$$Co^+(^3F) + H_2O \rightarrow CoH^+(^4\Phi) + OH + \Delta E_7 \quad (7)$$

$$Co^+(^3F) + H_2O \rightarrow CoH^+(^2\Delta) + OH + \Delta E_8 \quad (8)$$

3.3.2. $Ni^+(^2D) + H_2O$. Equations 9−14 represent the main ionic products of the reaction of $Ni^+(^2D)$ and H_2O. Table 6 lists the calculated ΔE values along with the experimental value given by Ryan and co-workers[10] for reaction 9, and the values for reactions 9, 11, and 13 extracted from the available thermodynamical data.[51]

$$Ni^+(^2D) + H_2O \rightarrow NiO^+(^4\Sigma) + H_2 + \Delta E_9 \quad (9)$$

$$Ni^+(^2D) + H_2O \rightarrow NiO^+(^2\Sigma) + H_2 + \Delta E_{10} \quad (10)$$

$$Ni^+(^2D) + H_2O \rightarrow NiOH^+(^3A'') + H + \Delta E_{11} \quad (11)$$

$$Ni^+(^2D) + H_2O \rightarrow NiOH^+(^1A') + H + \Delta E_{12} \quad (12)$$

$$Ni^+(^2D) + H_2O \rightarrow NiH^+(^3\Delta) + OH + \Delta E_{13} \quad (13)$$

$$Ni^+(^2D) + H_2O \rightarrow NiH^+(^1\Sigma) + OH + \Delta E_{14} \quad (14)$$

3.3.3. $Cu^+(^1S) + H_2O$. The corresponding equations for the main ionic products resulting in the reaction of $Cu^+(^1S)$ with H_2O are shown below. The various predicted ΔE values are listed in Table 7 along with the values reactions 15 and 19 extracted from the available thermodynamical data.[51]

$$Cu^+(^1S) + H_2O \rightarrow CuO^+(^3\Sigma) + H_2 + \Delta E_{15} \quad (15)$$

$$Cu^+(^1S) + H_2O \rightarrow CuO^+(^1\Delta) + H_2 + \Delta E_{16} \quad (16)$$

$$Cu^+(^1S) + H_2O \rightarrow HCuO^+(^2A'') + H + \Delta E_{17} \quad (17)$$

$$Cu^+(^1S) + H_2O \rightarrow CuOH^+(^2A'') + H + \Delta E_{18} \quad (18)$$

$$Cu^+(^1S) + H_2O \rightarrow CuH^+(^2\Sigma) + OH + \Delta E_{19} \quad (19)$$

3.4. The Stationary Points. In this section we examine the geometrical parameters calculated at the B3LYP/DZVP and B3LYP/TZVP+G(3df,2p) (in parentheses) levels of theory for the relevant minima and transition states on the potential energy surfaces for the reaction of the late transition metal cations with water.

Table 8 shows the geometrical parameters of the $M(OH_2)^+$ ion−molecule complexes. The low-lying triplet $Co(OH_2)^+$ ion−molecule shows several excited states lying very close in energy, which makes it quite hazardous to declare which of them is the ground state. First, Rosi and Bauschlicher assigned a $^3B_2$ ground state to this ion−molecule. Later, Tratchman and co-workers

(50) Moore, C. E. *Atomic Energy Levels*; National Bureau of Standards: Washington, DC, 1952; *Natl. Bur. Stand. Circular* **1959**, *2* (3), 467.

(51) Chase, M. W.; Davies, C. A.; Downey, J. R.; Frurip, D. J.; McDonald, R. A.; Syvened, A. N. *J. Phys. Chem. Ref. Data* **1985**, *14*, Suppl. N, 1 (JANAF Tables). (b) Gurvich, L. V.; Veyts, I. V.; Alcock, C. B. *Thermodynamic Properties of Individual Substances*, 4th ed.; Hemisphere: New York, 1989; Vol. 1, Part 2. (c) Armentrout, P. B. *Gas-Phase Inorganic Chemistry*; Russell, D. H., Ed.; Plenum Press: New York, 1989; p 1. (d) Armentrout, P. B.; Kickel, B. L. *Organometallic Ion Chemistry*; Freiser, B. S., Ed.; Kluwer: Dordrecht, 1996; p 1.

Table 6. Overall Energies for Reactions 9−14 at Several Levels of Theory[a]

method	ΔE_9	ΔE_{10}	ΔE_{11}	ΔE_{12}	ΔE_{13}	ΔE_{14}
B3LYP/DZVP	−2.544	−2.935	−2.336	−3.609	−2.964	−3.790
B3LYP/TZVP+G(3df,2p)	−2.630	−3.041	−2.390	−3.664	−3.136	−3.931
CCSD(T)//B3LYP	−2.708	−3.314	−2.655	−3.359	−3.465	−3.713
expt[51]	−2.30 ± 0.05		−2.68 ± 0.20		−3.44 ± 0.08	

[a] Energies given are in eV and for the various B3LYP levels of theory include ZPVE corrections calculated at the corresponding level of theory.

Table 7. Overall Energies for Reactions 15−19 at Several Levels of Theory[a]

method	ΔE_{15}	ΔE_{16}	ΔE_{17}	ΔE_{17}	ΔE_{19}
B3LYP/DZVP	−3.366	−3.949	−7.180	−3.146	−3.661
B3LYP/TZVP+G(3df,2p)	−3.623	−4.185	−7.431	−3.353	−3.910
CCSD(T)//B3LYP	−4.085	−5.717	−7.862	−3.832	−4.367
expt[51]	−3.42 ± 0.16				−4.21 ± 0.13

[a] Energies given are in eV and for the various B3LYP levels of theory include ZPVE corrections calculated at the corresponding level of theory.

Table 8. Geometrical Parameters of the Various $M(OH_2)^+$ Stationary Points on the B3LYP/DZVP and B3LYP/TZVP+G(3df,2p) Potential Energy Surfaces[a]

		B3LYP/DZVP			B3LYP/TZVP+G(3df,2p)		
metal	state	M−O	O−H	∠MOH	M−O	O−H	∠MOH
Co	$^3A_2$	2.005	0.971	126.0	1.999	0.965	126.0
Co	$^5B_2$	2.088	0.975	126.1	2.066	0.969	126.0
Ni	$^2A_1$	1.952	0.971	125.7	1.953	0.965	125.6
Ni	$^4A_2$				2.050	0.968	125.6
Ni	$^4A'$	2.086	0.975	123.3	2.055	0.968	125.3
Cu	$^1A_1$	1.946	0.971	125.7	1.946	0.965	125.7
Cu	$^3B_1$	2.096	0.979	126.2	2.035	0.971	126.0

[a] Bond lengths are reported in Å, bond angles in deg.

asigned a $^3A_2$ state as the ground state. Our B3LYP/TZVP+G(3df,2p) and CCSD(T)//B3LYP results are in accordance with this second work, but the B3LYP/DZVP level of theory predicts otherwise. At this latter level a $^3B_1$ state is predicted to be the ground state with the $^3A_2$ state lying 0.053 eV higher in energy and the $^3B_2$ state is higher still. No significant geometrical changes are observed between these two states. Based on our high-level calculations, and the results from Tratchman and coworkers, we have taken the $^3A_2$ state to be the ground state. The difference in the Co−O distance between the low-spin and high-spin states is only 0.067 Å.

The ground state of the $Ni(OH_2)^+$ metal cation−water complex corresponds to a well-described C_{2v} $^2A_1$ state, with a Ni−O distance of 1.953 Å. However, things are not so clear at the high-lying quartet state. The lowest-lying quartet, according to the B3LYP/TZVP+G(3df,2p) level of theory, is a $^4A_2$ state with C_{2v} symmetry. However, no C_{2v} minimum exists on the B3LYP/DZVP surface. That level of theory predicts a C_s minimum where the Ni lies 21.2° out of the HOH plane. It was also possible to characterize a C_s minimum at the B3LYP/TZVP+G(3df,2p) level of theory, but the out-of-plane angle is only 8.5° and the structure lies 0.006 eV higher in energy than the C_{2v} ground state.

Both high- and low-spin $Cu(OH_2)^+$ states have been found to be in accordance with all the methods and other theoretical data reported in the literature. The $^1A_1$ ground state has a Cu−O bond length of 1.945 Å, and the $^3B_1$ state has a 2.035 Å bond length at the B3LYP/TZVP+G(3df,2p) level of theory.

In all three of these late transition metal ion complexes the bond length corresponding to the high-spin state is longer than the low-spin one, as has been true along the row. Also, the tendency of complex M−O bond length shrinking continues in these late metals, as can be appreciated in Chart 1, which plots M−O bond distances for the high- and low-spin $M(OH_2)^+$ complexes for the first row transition metals.

Chart 1. M−O bond lengths for the $M(OH_2)^+$ ion−molecule complexes through the first row transition metal ions (B3LYP/DZVP values).

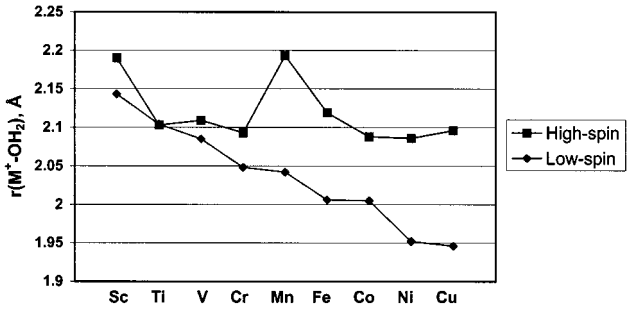

Table 9. Geometrical Parameters of the Various $TS1^+$ Transition States on the B3LYP/DZVP Potential Energy Surfaces[a]

metal	state	M−O	M−H(1)	O−H(1)	O−H(2)	∠MOH(1)
Co	^3A	1.736	1.498	1.717	0.979	51.4
Co	^5A	1.867	1.723	1.591	0.984	59.1
Ni	^2A	1.749	1.557	1.548	0.974	56.0
Ni	^4A	1.882	1.688	1.519	0.987	58.3
Cu	^3A	1.959	1.692	1.498	0.990	56.8

[a] Bond lengths are reported in Å, bond angles in deg.

Table 10. Geometrical Parameters of the Various $H(1)M^+OH(2)$ Stationary Points on the B3LYP/DZVP Potential Energy Surfaces[a]

metal	state	M−H(1)	M−O	O−H(2)	∠H(1)MO	∠MOH(2)
Co	^3A	1.468	1.694	0.981	87.5	123.1
Co	$^5A''$	1.570	1.738	0.982	145.9	134.7
Ni	$^2A''$	1.429	1.685	0.981	84.5	124.7
Ni	$^4A''$	1.498	1.897	0.989	122.0	126.2
Ni	$^4A'$	1.513	1.872	0.982	106.6	186.9
Cu	^3A	1.527	1.903	0.989	118.4	125.0

[a] Bond lengths are reported in Å, bond angles in deg.

The first hydrogen transfer from oxygen to the metal is characterized by the $TS1^+$ structures. Note that $TS1^+$ is a transition state associated with oxidative addition of an OH bond to the metal center. Geometrical parameters are listed in Table 9. While the M−O distance in the high-spin states is seen to increase in moving from left to right through the first row transition metals, a tendency to decrease this bond distance is observed for the low-spin structures.

Table 10 shows the geometrical data for the HM^+OH minima; almost all of them have C_s symmetry. This intermediate has been well-characterized for all the reactions studied by our group, except for the singlet copper surface, where it has not been possible to obtain this minimum even at high levels of theory. The nonexistence of a singlet HCu^+OH intermediate is

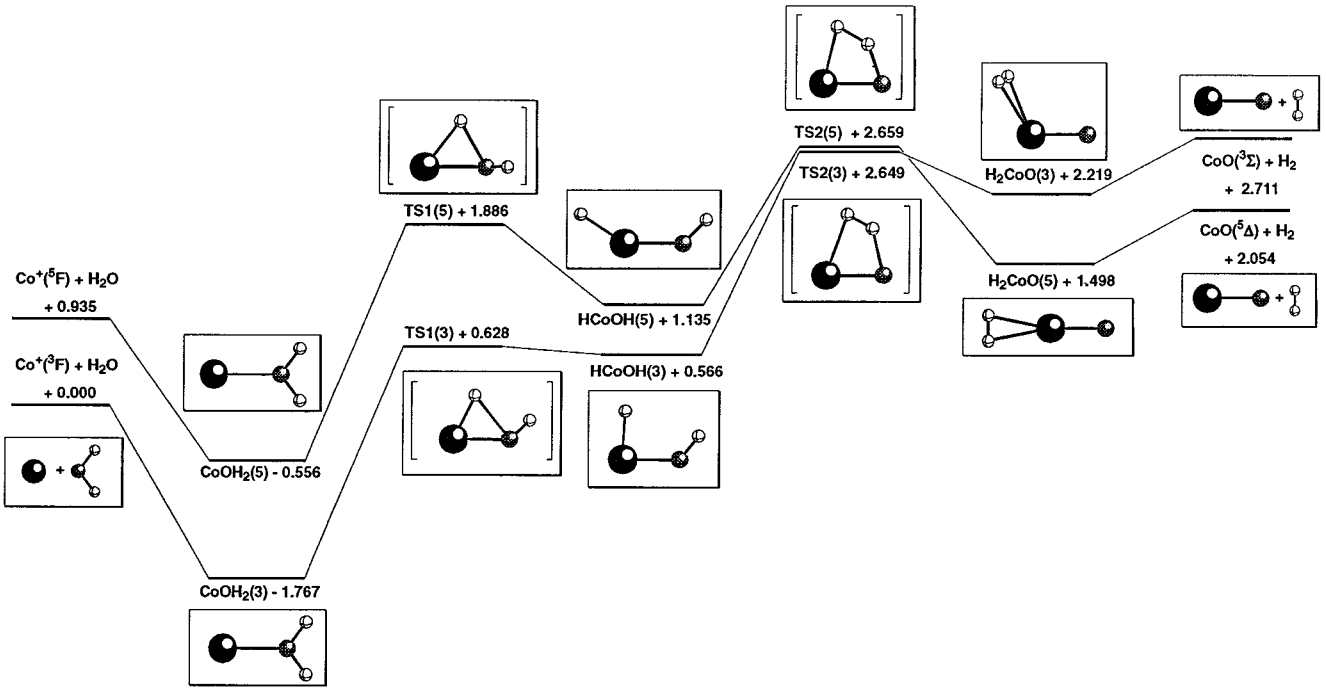

Figure 1. B3LYP/DZVP potential energy surface following the $Co^+ + H_2O \rightarrow CoO^+ + H_2$ reaction path. Energies given are in eV and are relative to the separated ground state reactants, $Co^+(^3F) + H_2O$.

Chart 2. M−H bond lengths for the HM^+OH intermediates through the first row transition metal ions (B3LYP/DZVP values).

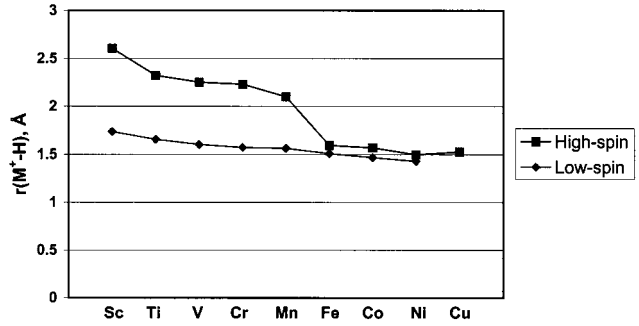

reasonable, because the valence space on the Cu atom would be filled with lone pairs and Cu−O bonding, leaving no opprotunities for Cu−H interaction. Note also that these intermediates in the high-spin Ni and Cu cases have very long M−O bonds in comparison with the rest of the row. Comparing all other HM^+OH intermediates, the differences between the low- and high-spin M−H distances are minimal in the Fe−Ni metals, which was not the case for the earlier metals (see Chart 2). The low-spin cases follow the expected trend, with the M−H bond distance decreasing from Sc to Ni. In the high-spin cases this decreasing trend is only broken in the Cu moiety, but its M−H bond length is only 0.029 Å larger than that of HNi^+-OH.

The second transition state, $TS2^+$, is a four-center transition state with an incipient H−H bond. As can be seen in Table 11, the low-spin isomers of these transition states show H−H distances that are still quite long for bonds. The tendency seen earlier is continued; that is, these bond distances tend to be shorter as we go through the row.

For the early transition metal cations we found that the M−O distance in low-spin $TS2^+$ is closer to the HM^+OH value than that to the following $(H_2)MO^+$ species, for the middle transition metal cations these distances were similar, and for the late transition metals the M−O distance at the second transition state is closer to that of the ion−molecule complex than to the previous intermediate.

Table 11. Geometrical Parameters of the Various $TS2^+$ Transition States on the B3LYP/DZVP Potential Energy Surfaces

metal	state	M−H(1)	M−O	O−H(2)	H(1)−H(2)	∠H(1)MO	∠MOH(2)
Co	$^3A'$	1.949	1.716	1.451	0.852	70.4	77.2
Co	$^5A''$	1.748	1.752	1.257	1.063	76.2	71.4
Ni	$^2A'$	1.825	1.762	1.553	0.833	75.6	69.8
Ni	$^2A''$	1.702	1.893	1.409	0.953	76.8	62.9
Ni	$^4A''$	1.688	1.890	1.359	0.975	75.6	64.5
Ni	$^4A'$	1.781	1.879	1.320	0.976	72.3	68.6
Cu	$^1A''$	1.763	1.882	1.380	0.931	73.6	66.2
Cu	$^3A''$	1.742	1.910	1.313	0.963	71.4	67.9

[a] Bond lengths are reported in Å, bond angles in deg.

For the high-spin four-centered Sc−Cr transition metal $TS2^+$ transition states we observed an almost fully formed H−H bond and very long M−H and O−H bond distances. For the high-spin iron transition state we found a H−H bond 0.199 Å longer than the respective bond in the chromium complex, and M−H and O−H bonds appreciably shorter than the previous ones. For iron also the O−H distance was shorter than its low-spin O−H distance. For the late transition metals the low-spin M−H and O−H distances are slightly longer than the high-spin ones, and now shorter H−H bond lengths are observed in the low-spin transition states than in the high-spin ones.

The final stationary points located on our potential energy surfaces were the $(H_2)MO^+$ hydrogen molecule metal oxide adducts illustrated in Table 12. As we have discussed previously,[2] this minimum should be considered an ion−molecule complex. The M−H bond length in these complexes is seen to shorten slightly in moving from Sc through to Cu in both the high- and low-spin cases. The only exception to this is the low-spin $(H_2)FeO^+$ case in which the H−Fe bond is significantly shorter than those found in the other $(H_2)MO^+$ moieties.

For these three late transition metal low-spin systems also there is an interaction between the singly occupied d orbital of the metal and the σ^*_{H-H} orbital (shown in Figure 2 of ref 2). It

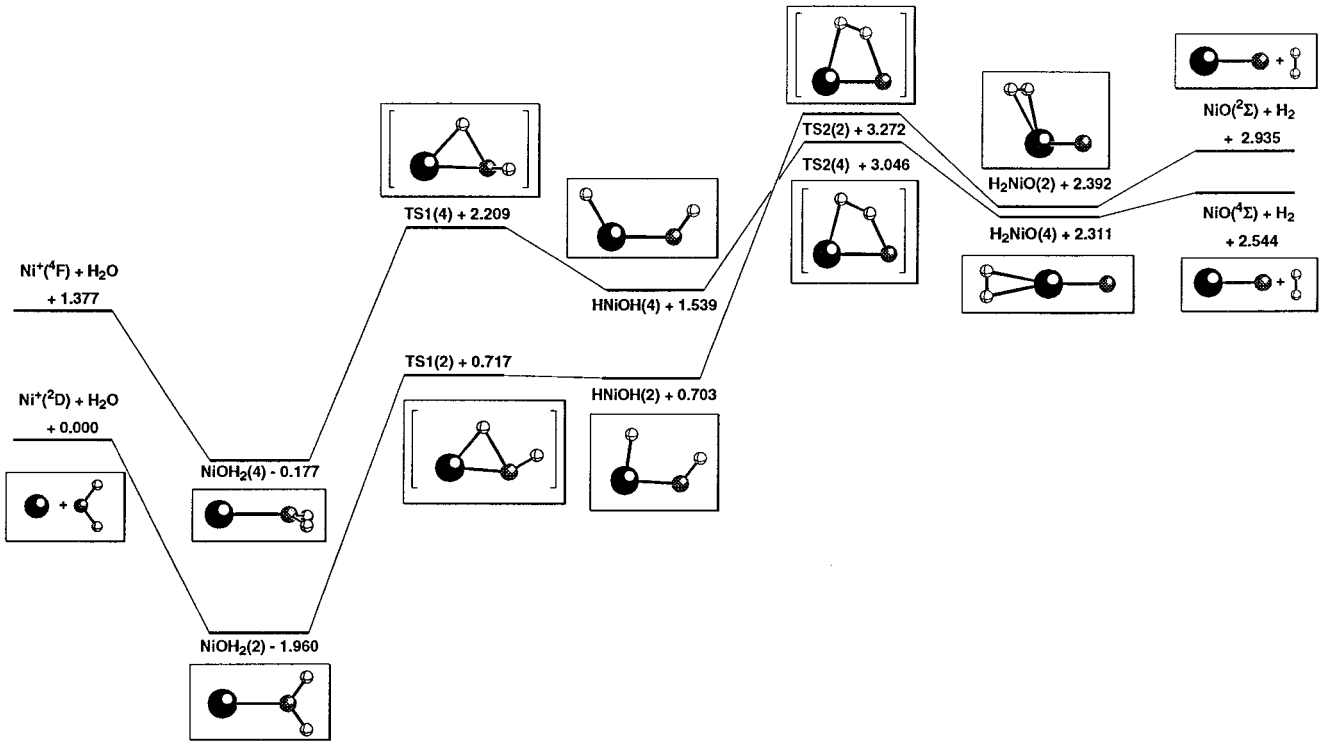

Figure 2. B3LYP/DZVP potential energy surface following the $Ni^+ + H_2O \rightarrow NiO^+ + H_2$ reaction path. Energies given are in eV and are relative to the separated ground state reactants, $Ni^+(^2D) + H_2O$.

Table 12. Geometrical Parameters of the Various $(H_2)MO^+$ Stationary Points on the B3LYP/DZVP Potential Energy Surfaces[a]

metal	state	M−O	M−H(1)	M−H(2)	H−H	∠(H2)MO
Co	$^3A''$	1.687	1.879	1.879	0.774	116.3
Co	$^5A''$	1.657	1.945	1.945	0.767	180.0
Ni	$^2A''$	1.697	1.834	1.834	0.777	115.4
Ni	$^2A'$	1.814	1.810	1.810	0.776	180.0
Ni	$^4A'$	1.781	1.841	1.841	0.773	180.0
Ni	$^4A''$	1.762	1.857	1.857	0.776	180.0
Cu	^1A	1.788	1.810	1.810	0.775	180.0
Cu	$^3A''$	1.814	1.798	1.798	0.776	180.0

[a] Bond lengths are reported in Å, bond angles in deg. Note that $(H_2)MO$ refers to the angle formed by the O atom, the M atom, and the center of the H−H bond.

is significantly lower than for the previous metals (5.09 kcal/mol for iron vs 2.35, 2.90, and 2.22 kcal/mol respectively for cobalt, nickel, and copper). The back-donation from the σ_{H-H} orbital to the metal's s orbital should also be remarked upon in these three metal systems. The NBO analysis gives that donation a value of 7.91 kcal/mol in the case of Co, 15.36 kcal/mol in the case of Ni, and 15.40 kcal/mol in the case of Cu, which can be compared to the value of 11.77 kcal/mol in the iron case.

3.5. Potential Energy Surfaces. Armentrout and co-workers in investigating the $Co^+ + H_2O$ reaction[8] did not observe any evidence of CoO^+ formation. They only found evidence of CoH^+ and $CoOH^+$ formation even though the thermodynamic threshold found for these ions is higher than for that of CoO^+ (see energetics in Table 5). Several other experimental works on the cobalt systems have also shown that even if the reverse reaction is clearly exothermic it is very inefficient, so detailed PES calculations have been required to clarify the reasons for this inefficiency.[7,10] Such calculations are sumarized in Figures 1−3, where the potential energy surfaces starting from the $M^+ + OH_2$ separated reactants and leading to the products $MO^+ + H_2$ for the high- and low-spin states at the B3LYP/DZVP level of theory for Co^+, Ni^+, and Cu^+ are shown respectively. Chart 3 shows the evolution of the high-/low-spin relative energies

Chart 3. Evolution of the high-/low-spin $M^+ + H_2O$ relative energies with respect to the most stable $M^+ + H_2O$ system across the row. Except for Fe, where CCSD(T)// B3LYP values were used, B3LYP/DZVP predicted energies are shown.

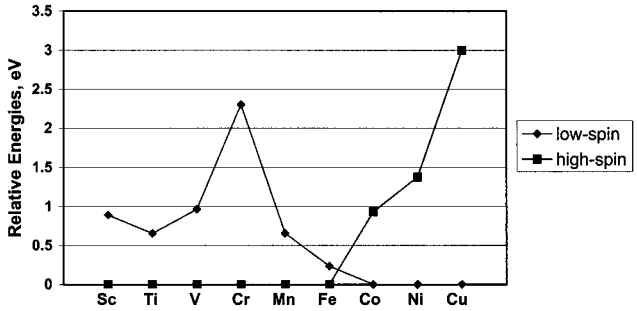

across the row. The graphs given in this section are energies predicted at the B3LYP/DZVP level of theory except for the notoriously difficult Fe case, for which the CCSD(T)//B3LYP level of theory was used.

Generally the surfaces for the reactions of Co^+, Ni^+, and Cu^+ are similar to those we have reported earlier,[2−4] with the first step being the formation of the $M(OH_2)^+$ ion−molecule complex. Through $TS1^+$, one hydrogen atom is passed from oxygen to the metal, leading to the HM^+OH intermediate. Note that on the low-spin surfaces the HCo^+OH intermediate lies only 0.062 eV below the associated $TS1^+$ and the HNi^+OH minimum a mere 0.014 eV. As discussed earlier, no HCu^+OH intermediate exists on the singlet surface. Along the row the relative energy of this barrier on the low-spin surface has augmented in relative energy somewhat, with the exception of Cr which shows an especially large low-spin barrier. The relative energies of the high-spin $TS1^+$ stationary points, too, increase in moving from left to right along the row, as can be seen in Chart 4.

Armentrout and co-workers[8] note that qualitatively the first

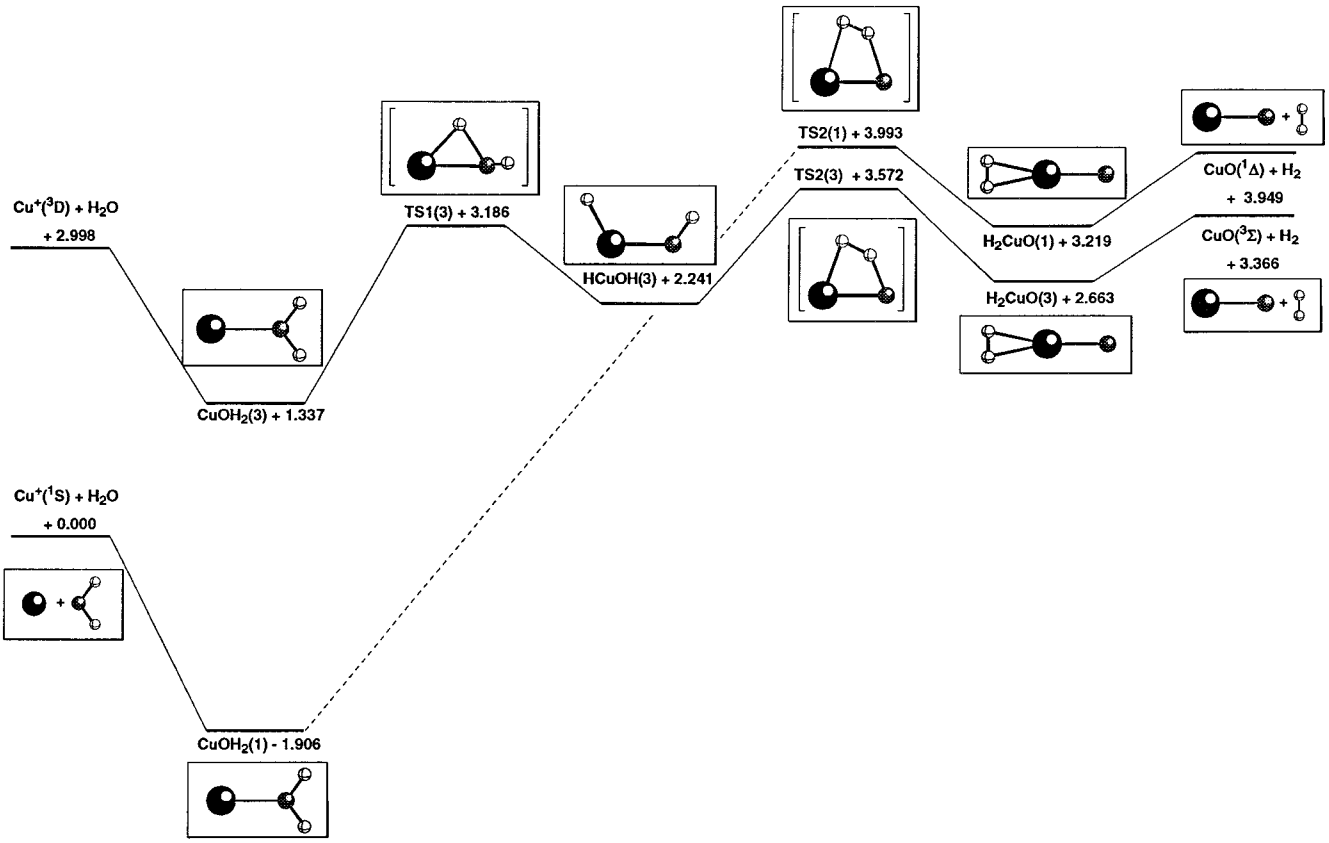

Figure 3. B3LYP/DZVP potential energy surface following the $Cu^+ + H_2O \rightarrow CuO^+ + H_2$ reaction path. Energies given are in eV and are relative to the separated ground state reactants, $Cu^+(^1S) + OH_2$.

Chart 4. Evolution of the high-/low-spin $TS1^+$ relative energies with respect to the most stable $M^+ + H_2O$ system across the row. Except for Fe, where CCSD(T)//B3LYP values were used, B3LYP/DZVP predicted energies are shown.

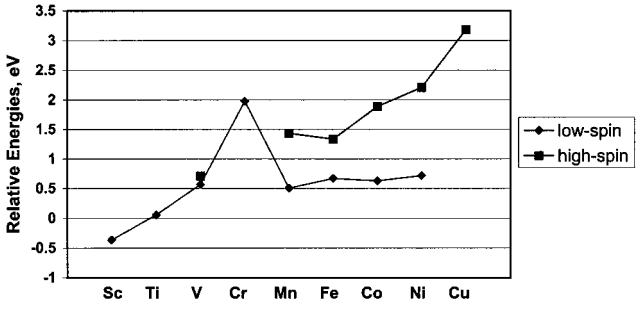

barrier corresponding to the low-spin $TS1^+$ in the $Co^+ + H_2O$ reaction should not be higher than the energy of $CoOD^+ + D$. Our results are in accordance with this since we obtain a value of 2.070 eV for reaction 5 (see Table 5), and predict that $TS1^+$ represents a barrier of 0.628 eV (see Figure 1).

The second barrier is associated with $TS2^+$. Through the early and middle transition metals, the gap between the high- and low-spin $TS2^+$ stationary points has decreased along the row significantly. We find now that for cobalt the high- and low-spin states of $TS2^+$ are almost energetically degenerate and for nickel and copper there is an inversion, with the high-spin transition states being lower in energy. Chart 5 plots the relative energies of these stationary points along the row.

It should be pointed out that the lowest barrier for the doublet $TS2^+$ in the Ni case is a $^2A'$ state, while the HNi^+OH species has a $^2A''$ ground state. We give the lower barrier because movement of the H atoms should be facile, opening the

Chart 5. Evolution of the high-/low-spin $TS2^+$ relative energies with respect to the most stable $M^+ + H_2O$ system across the row. Except for Fe, where CCSD(T)//B3LYP values were used, B3LYP/DZVP predicted energies are shown.

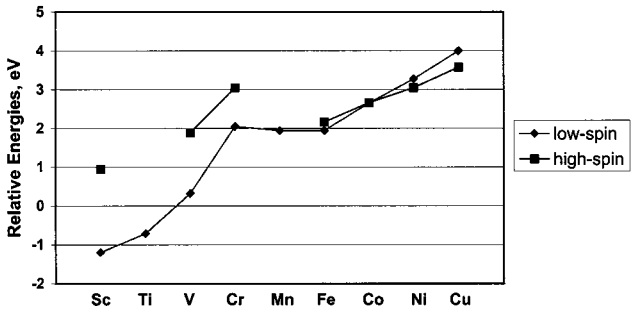

possibility of dropping into C_1 where the states can mix. The $^2A''$ state lies 0.121 eV above the $^2A'$ $TS2^+$.

After overcoming this maximum we fall to the final intermediate found on the reaction path, the $(H_2)MO^+$ ion−molecule complex. For the low-spin cases this complex bonding becomes stronger from Co (0.492 eV) to Cu (0.730 eV), continuing the observed trend. For the high-spin complexes we found that there is a minimum in the bond strength at the vanadium complex, and afterward this bond becomes stronger in moving from left to right along the row. This nice picture is broken by nickel, in which the $^4A'$ ground-state complex is bound by only 0.233 eV, 0.120 eV weaker than the vanadium complex.

Experimental results from Armentrout and co-workers studying the reverse reaction, $CoO^+ + D_2$,[8] found a barrier to reaction of 0.75 ± 0.04 eV. As seen in Figure 1, our B3LYP/DZVP level of theory predicts a barrier 0.605 eV above the $CoO^+ + D_2$ asymptote energy.

Chart 6. Evolution of the high-/low-spin $MO^+ + H_2$ relative energies with respect to the most stable $M^+ + H_2O$ system across the row. Except for Fe, where CCSD(T)//B3LYP values were used, B3LYP/DZVP predicted energies are shown.

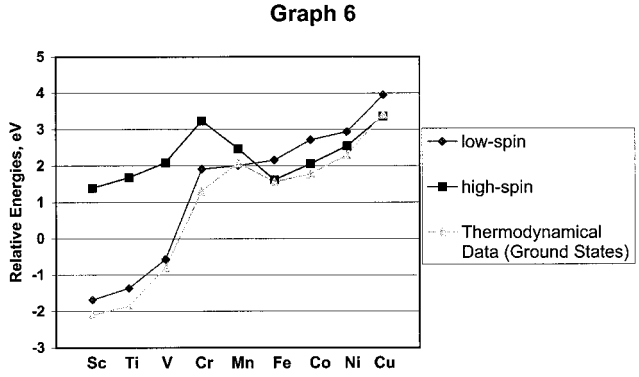

From the $(H_2)MO^+$ intermediate, the loss of H_2 proceeds without transition state to the corresponding high- and low-spin MO^+ and H_2 molecules. The relative energies of the $MO^+ + H_2$ products with respect to the most stable $M^+ + H_2O$ system are plotted in Chart 6.

For these metals clearly the surface crossing takes place near the $TS2^+$ transition state, that is, at the exit channel, while this crossing was observed at the entrance channel for the Sc−Mn metals and at both sites for iron.

Equilibrium geometry parameters for the various reaction products are given in Table 13.

4. Conclusions

The reactions of Co^+, Ni^+, and Cu^+ with water have been investigated in detail completing the study of the reactivity of the first row transition metals. Both the low- and high-spin potential energy surfaces have been characterized at the B3LYP/DZVP level of theory. Energy differences between key low- and high-spin species and total reaction energies for the possible products have been predicted at even higher levels of theory including B3LYP/TZVP+G(3df,2p) and CCSD(T)/TZVP+G(3df,2p)//B3LYP/TZVP+G(3df,2p). From these data, the following conclusions are drawn:

1. The expected trend for the $M(OH_2)^+$ ion−molecule dissociation energies has been well described through the row. B3LYP/TZVP+G(3df,2p) appears to be the best method fitting the experimental data.

2. Similar performance from the B3LYP/TZVP+G(3df,2p) and CCSD(T)//B3LYP levels of theory was obtained in comparison with experimental data of high-/low-spin splittings on the metal cations.

3. Whereas the only exothermic products of the $M^+ + H_2O$ reaction for M = Sc to V were $MO^+ + H_2$ with exothermicity decreasing from Sc to V, said reactions were endothermic for M = Cr to Cu with endothermicity increasing through the series.

4. As in the $Fe^+ + H_2O$ system, less difference between the high- and low-spin structures than in the early transition metal systems was observed for the late transition metals. The reason for this is that the high-spin Fe^+ to Cu^+ cations have at least one set of paired electrons while the Sc^+ to Mn^+ high-spin cations do not.

5. Both high- and low-spin potential energy surfaces cross once in the entrance channel for Sc^+ to Mn^+. Two crossings were observed, at the entrance and exit channels, on the Fe^+ potential energy surfaces. Finally, the surfaces of Co^+ to Cu^+ demonstrate one crossing, near the exit channel.

Table 13. Equilibrium Geometry Parameters for the Various $M^+ + OH_2$ Reaction Products at the B3LYP/DZVP and B3LYP/TZVP+G(3df,2p) Levels of Theory[a]

			B3LYP/DZVP			B3LYP/TZVP+G(3df,2p)		
product	metal	state	M−O	M−H	angle	M−O	M−H	angle
MO^+	Co	$^3\Sigma$	1.705			1.705		
		$^5\Delta$	1.648			1.634		
	Ni	$^2\Delta$	1.687			1.681		
		$^4\Delta$	1.643			1.638		
	Cu	$^1\Delta$	1.786			1.775		
		$^3\Sigma$	1.807			1.797		
MH^+	Co	$^2\Delta$	1.461			1.467		
		$^4\Phi$	1.520			1.535		
	Ni	$^1\Sigma$		1.414		1.415		
		$^3\Delta$		1.474		1.485		
	Cu	$^2\Delta$		1.488		1.488		
HMO^+	Co	$^3A''$	1.615	1.451	84.7	1.599	1.455	85.7
		$^4A''$	1.601	1.475	81.9	1.585	1.485	83.4
	Cu	$^2A''$	2.047	1.508	178.3	1.969	1.501	178.6
MOH^+	Co	$^2A'$	1.758	0.980	126.3	1.748	0.972	125.0
		$^4A'$	1.731	0.978	126.6	1.726	0.969	125.8
	Ni	$^1A'$	1.697	0.979	124.2	1.688	0.972	122.4
		$^3A''$	1.714	0.979	129.4	1.708	0.971	127.8
	Cu	$^2A''$	1.816	0.984	124.1	1.808	0.977	123.3

[a] Bond lengths are reported in Å, bond angles in deg.

Acknowledgment. A.I. and J.E.F. thank the Basque Government (Eusko Jaurlaritza) for a grant. Financial support from The University of the Basque Country (Euskal Herriko Unibertsitatea) Grant No. 203.215-G50/98, the Spanish DGICYT Grant No. PB96/1524, and the Provincial Government of Gipuzkoa (Gipuzkoako Foru Aldundia) is gratefully acknowledged.

JA991657R